

# Boundary of quantum evolution under decoherence

Navin Khaneja<sup>†§</sup>, Burkhard Luy<sup>†</sup>, and Steffen J. Glaser<sup>†</sup>

<sup>†</sup>Division of Applied Sciences, Harvard University, Cambridge, MA 02138; and <sup>†</sup>Institute for Organic Chemistry and Biochemistry, Technische Universität München, 85747 Garching, Germany

Edited by Alfred G. Redfield, Brandeis University, Waltham, MA, and approved August 13, 2003 (received for review June 28, 2003)

**Relaxation effects impose fundamental limitations on our ability to coherently control quantum mechanical phenomena. In this article, we use principles of optimal control theory to establish physical limits on how closely a quantum mechanical system can be steered to a desired target state in the presence of relaxation. In particular, we explicitly compute the maximum amplitude of coherence or polarization that can be transferred between coupled heteronuclear spins in large molecules at high magnetic fields in the presence of relaxation. Very general decoherence mechanisms that include cross-correlated relaxation have been included in our analysis. We give analytical characterization for the pulse sequences (control laws) that achieve these physical limits and provide supporting experimental evidence. Exploitation of cross-correlation effects has recently led to the development of powerful methods in NMR spectroscopy to study very large biomolecules in solution. For two heteronuclear spins, we demonstrate with experiments that cross-correlated relaxation optimized pulse (CROP) sequences provide significant gains over the state-of-the-art methods. It is shown that despite large relaxation rates, coherence can be transferred between coupled spins without any loss in special cases where cross-correlated relaxation rates can be tuned to autocorrelated relaxation rates.**

The control of quantum ensembles has many applications, ranging from coherent spectroscopy to quantum information processing. In practice, the quantum system of interest interacts with its environment, which leads to the phenomenon of relaxation. This results in signal loss and ultimately limits the range of applications. Relaxation is also a major road block standing in the way of practical quantum computing. Manipulating quantum systems in a manner that minimizes relaxation losses is a fundamental challenge of utmost practical importance. What is the ultimate limit on how close an ensemble of quantum systems can be steered from an initial state to a desired target state in the presence of relaxation? Until now there existed no theory that answers this question. This situation is comparable to the time before the fundamental efficiency limits of heat engines were known: More than 100 years after the invention of the steam engine, the physical limits for the maximum amount of work a steam engine could produce were unclear, despite decades of advances in its design. “The theory of its operation is rudimentary and attempts to improve its performance are still made in an almost haphazard way” (1). Of course, the maximum efficiency of a heat engine is not given by the cleverness of the engineer who attempts to build such a machine, but by the fundamental law of thermodynamics as captured in Carnot’s Theorem.

In this article we derive fundamental limits on how close an ensemble of nuclear spins can be driven from its initial state to a desired target state in the presence of relaxation. In particular, we derive the maximum efficiency of polarization and coherence transfer between coupled nuclear spins. Such coherence transfer operations are important in high-resolution NMR spectroscopy (2, 3). In structural biology, NMR spectroscopy is an important technique that allows one to determine the structure of biological macromolecules, such as proteins, in aqueous solution. With increasing size of molecules or molecular complexes, the rotational tumbling of the molecules becomes slower and leads to increased relaxation losses. When these relaxation rates become

comparable to the spin–spin couplings, the efficiency of coherence transfer is considerably reduced, leading to poor sensitivity and increased measurement times. Recent advances have made it possible to significantly extend the size limit of biological macromolecules amenable to study by liquid-state NMR (4–7). These techniques take advantage of the phenomenon of cross-correlated relaxation, which represents interference effects between two different relaxation mechanisms (8–13). Until now, it was not clear if further improvements can be made and what is the physical limit for the coherence transfer efficiency between coupled spins in the presence of cross-correlated relaxation.

In this article, we give analytical expressions for this maximum achievable coherence transfer efficiency for two coupled heteronuclear spins under very general decoherence mechanisms that include cross-correlated relaxation. We describe the optimal pulse sequences that achieve this efficiency and provide experimental data that support these results. In the general case of cross-correlated relaxation, we demonstrate substantial improvement over previously known sequences in NMR spectroscopy. It should be noted that the optimal transfer efficiency reported here applies to the case where the resonance frequencies of a single spin pair (*I* and *S*) are known. However, the presented approach will also make it possible to derive optimal broadband transfer schemes for a given range of resonance frequencies.

We also show theoretically that in the limit where the cross-correlated relaxation rates become identical to the autocorrelated relaxation rates, lossless transfer of coherence is possible between coupled spins. For an isolated spin pair in an isotropically tumbling molecule, this limit can be reached if the interfering interactions are axially symmetric and if the symmetry axes and the size of the interactions coincide (4, 12). Although this is not the generic case, it can be approached by many systems of practical interest (4, 6), and it may be feasible to construct molecules for quantum information processing in which a complete match is possible.

## Theory

Let  $\rho$  denote the density operator of a quantum mechanical system coupled to a bath. Under the assumption of Markovian dynamics for the system of interest (very short correlation times with the bath) (14), the most general form for the evolution of the system density operator  $\rho$  takes the form

$$\frac{d}{dt}\rho = -i[\mathbf{H}, \rho] + L_D[\rho] \quad [1]$$

$$L_D[\rho] = \frac{1}{2} \sum_{k,l=1}^M a_{k,l} L_{F_k F_l}[\rho] \quad [2]$$

$$L_{F_k F_l}[\rho] = [F_k, \rho F_l^\dagger] + [F_k \rho, F_l^\dagger], \quad [3]$$

This paper was submitted directly (Track II) to the PNAS office.

Abbreviations: CSA, chemical shift anisotropy; DD, dipole–dipole; CROP, cross-correlated relaxation optimized pulse.

<sup>§</sup>To whom correspondence should be addressed. E-mail: navin@hrl.harvard.edu.

© 2003 by The National Academy of Sciences of the USA

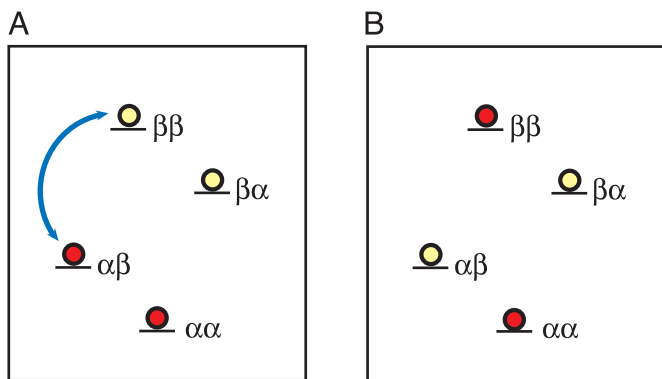


**Fig. 1.** Selective population inversion of the energy levels  $\alpha\beta$  and  $\beta\beta$ , corresponding to a transfer of polarization  $I_z$  (A) to longitudinal two-spin order  $2I_zS_z$  (B).

where  $\mathbf{H}$  is the systems Hamiltonian and generates unitary evolution. All nonunitary relaxation dynamics is accounted for by  $L_D$ . The Hermitian coefficient matrix  $A \equiv \{a_{k,l}\}$  contains the information about physical relaxation parameters (lifetimes, relaxation rates) and  $F_k$  denotes operators representing various relaxation mechanisms (14).

We now consider an isolated heteronuclear spin system consisting of two coupled spins  $1/2$ , denoted  $I$  (e.g.,  $^1\text{H}$ ) and  $S$  (e.g.,  $^{15}\text{N}$ ). To fix ideas, we first address the problem of selective population inversion of two energy levels (e.g.,  $\alpha\beta$  and  $\beta\beta$ ) as shown in Fig. 1. This is a central step in high-resolution multi-dimensional NMR spectroscopy and corresponds to the transfer of an initial state  $I_z$ , representing polarization on spin  $I$ , to the target state  $2I_zS_z$  representing longitudinal two-spin order. We now consider the slow tumbling regime (the so-called spin diffusion limit) (2), which applies to macromolecules at high magnetic fields, where the correlation time of the molecular tumbling is much shorter than the inverse of the resonance frequencies of spins  $I$  and  $S$ . In this limit, longitudinal relaxation rates are negligible compared with transverse relaxation rates for an isolated heteronuclear spin system consisting of two coupled spins  $1/2$ , where the two principle relaxation mechanisms are dipole–dipole (DD) relaxation and relaxation due to the chemical shift anisotropy (CSA) of spins  $I$  and  $S$ . Hence, both the initial state ( $I_z$ ) and final state ( $2I_zS_z$ ) are long-lived. However, the transfer between these two states requires the creation of coherences that in general are subject to fast transverse relaxation. In a double rotating frame chosen specifically for the pair of spins under discussion, the above set of equations (Eqs. 1–3) take the following form (Eq. 4), where  $F_1 = 2I_zS_z$ ,  $F_2 = I_z$ ,  $F_3 = S_z$ , and we assume  $a_{23} = 0$  because in the present application interference terms between the CSA of spins  $I$  and  $S$  have no effect on the involved density operator terms (see below):

$$\begin{aligned} \dot{\rho} = & \pi J[-i2I_zS_z, \rho] + \pi k_{\text{DD}}[2I_zS_z, [2I_zS_z, \rho]] \\ & + \pi k_{\text{CSA}}^I[I_z, [I_z, \rho]] + \pi k_{\text{CSA}}^S[S_z, [S_z, \rho]] \\ & + \pi k_{\text{DD/CSA}}^I[2I_zS_z, [I_z, \rho]] + \pi k_{\text{DD/CSA}}^S[2I_zS_z, [S_z, \rho]], \end{aligned} \quad [4]$$

where  $J$  is the heteronuclear coupling constant. The rates  $k_{\text{DD}}$ ,  $k_{\text{CSA}}^I$ , and  $k_{\text{CSA}}^S$  represent autocorrelated relaxation rates due to DD relaxation, CSA relaxation of spin  $I$ , and CSA relaxation of spin  $S$ , respectively. The rates  $k_{\text{DD/CSA}}^I$  and  $k_{\text{DD/CSA}}^S$  represent cross-correlation rates of spin  $I$  and  $S$  caused by interference effects between DD and CSA relaxation. Unconventional  $\pi$  factors in front of the relaxation rates results in concise expres-

sions of optimal transfer efficiency later. The relaxation rates depend on various physical parameters, such as the gyromagnetic ratios of the spins, the internuclear distance, the CSA tensors, the strength of the magnetic field, and the correlation time of the molecular tumbling (2, 11).

Let the initial density operator be  $\rho(0) = A$  and denote the density operator at time  $t$  by  $\rho(t)$ . The maximum efficiency of transfer between  $A$  and target operator  $C$  is defined as the largest possible value of  $\text{trace}(C^\dagger \rho(t))$  for any time  $t$  (3) (by convention operators  $A$  and  $C$  are normalized).

The main result of this article is as follows. The maximal efficiency of transfer between the operators  $I_z$  and  $2I_zS_z$  depends only on the scalar coupling constant  $J$  and the net autocorrelated and cross-correlated relaxation rates of spin  $I$ , given by  $k_a = k_{\text{DD}} + k_{\text{CSA}}^I$  and  $k_c = k_{\text{DD/CSA}}^I$ , respectively. Here the rates  $k_a$  and  $k_c$  are a factor of  $\pi$  smaller than in conventional definitions of the rates, e.g.,  $k_a = 1/(\pi T_2)$  if  $T_2$  is the transverse relaxation rate in the absence of cross-correlation effects (15). The physical limit  $\eta$  of the maximal transfer efficiency is given by

$$\eta = \sqrt{1 + \zeta^2} - \zeta, \quad [5]$$

where

$$\zeta = \sqrt{\frac{k_a^2 - k_c^2}{J^2 + k_c^2}}. \quad [6]$$

The derivation of the maximal efficiency rests on the basic principles of optimal control theory (16, 17) (for details, see *Supporting Methods*, which is published as supporting information on the PNAS web site). The optimal transfer scheme (CROP, cross-correlated relaxation optimized pulse) has two constants of motion. If  $l_1(t)$  and  $l_2(t)$  denote the two-dimensional vectors ( $\langle I_x \rangle(t)$ ,  $\langle I_y \rangle(t)$ ) and ( $\langle 2I_xS_z \rangle(t)$ ,  $\langle 2I_yS_z \rangle(t)$ ), respectively, then throughout the transfer process the ratio of the magnitudes of the vectors  $l_2$  and  $l_1$  is maintained constant at  $\eta$ . Furthermore, the angle  $\gamma^*$  between  $l_1$  and  $l_2$  is constant throughout. The two constants of motion of the optimal transfer scheme determine the amplitude and phase of the rf field at each point in time and explicit expressions for the optimal pulse sequence can be derived (see *Supporting Methods*).

We now consider two important limiting cases of this problem:

(i) In the case when  $k_a > 0$  and  $k_c = 0$  (no cross-correlated relaxation), the optimal efficiency  $\eta$  is equal to  $\sqrt{1 + (k_a^2/J^2)} - (k_a/J) < 1$  (see curve for  $k_c/k_a = 0$  in Fig. 2A) and the optimal angle  $\gamma^*$  is  $\pi/2$  (15).

(ii) In the limit where the cross-correlation coefficient  $k_c/k_a$  approaches 1, the optimal transfer efficiency  $\eta$  approaches 1 (see curve for  $k_c/k_a = 1$  in Fig. 2), and  $\gamma^*$  approaches  $\pi$ . Surprisingly, in this case using optimal control it is possible to transfer coherence without any loss in the presence of relaxation. In the limit of large relaxation rates  $k_a$ , this relaxation-optimized transfer mechanism gains up to 100% compared with state-of-the-art transfer schemes.

The optimal transfer scheme is best illustrated by decomposing the initial operator  $I_z$  as a sum of the two single-transition operators  $I_zS^\alpha = I_z/2 + I_zS_z$  and  $I_zS^\beta = I_z/2 - I_zS_z$  (2). The transverse components  $I_xS^\alpha$ ,  $I_yS^\alpha$  and  $I_xS^\beta$ ,  $I_yS^\beta$  relax with rates  $k_a + k_c$  and  $k_a - k_c$ , respectively. When  $k_c/k_a$  approaches 1, the transverse single-transition operators  $I_xS^\beta$  and  $I_yS^\beta$  do not relax. The optimal pulse sequence in this case reduces to selectively inverting  $I_zS^\beta$  to  $-I_zS^\beta$  by weak rf irradiation at the frequency ( $-J/2$ ) of the slowly relaxing multiplet component. Such selective inversions have been performed in the past for various applications, including the selective measurement of relaxation rates (11, 20–23). Because the component  $I_zS^\alpha$ , which we do not want to invert, has a large transverse relaxation rate given by  $k_a + k_c$ , it is possible to carry out the selective inversion process

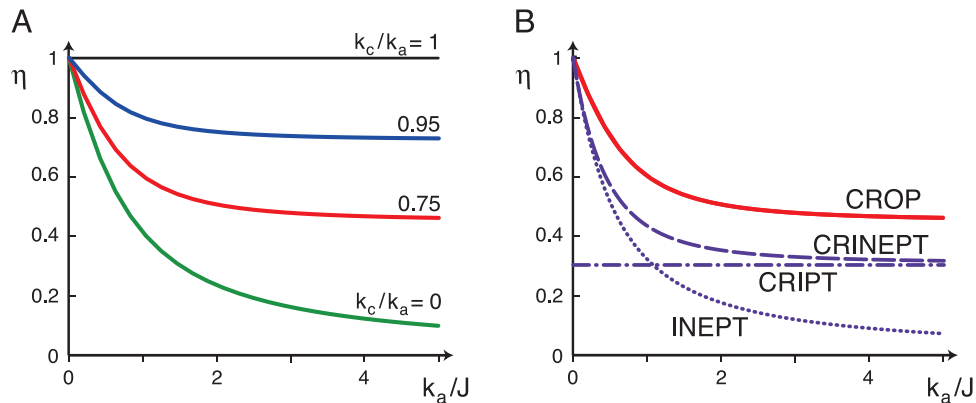


**Fig. 2.** (A) Physical limits of the transfer efficiency  $\eta$  as a function of  $k_a/J$  for  $k_c/k_a = 0$ ,  $k_c/k_a = 0.75$ ,  $k_c/k_a = 0.95$ , and  $k_c/k_a = 1$ . (B) For the case  $k_c/k_a = 0.75$ , the theoretical bound of the transfer efficiency (CROP, solid curve) is compared with the transfer efficiency of conventional transfer schemes [INEPT (18), dotted curve; CRIPT (19), dash-dotted curve; and CRINEPT (7), dashed curve].

much more rapidly than in the absence of relaxation. In Fig. 3, optimal trajectories of the two multiplet components are shown for several cross-correlation coefficients  $k_c/k_a$  and  $k_a = J$ .

In Fig. 4, the optimal rf amplitude and irradiation frequency of a CROP sequence is shown as a function of time for the case  $k_c/k_a = 0.75$  and  $k_a = J$ . Although the ideal sequence has a long duration, most of the transfer occurs in a relatively short time window, outside of which the rf amplitude is vanishingly small.

The transfer efficiency  $\eta$  is shown in Fig. 2A for several ratios  $k_c/k_a$  as a function of the autocorrelated relaxation rate  $k_a/J$ . For the case  $k_c/k_a = 0.75$ , the physical limit of the transfer efficiency is compared in Fig. 2B to the transfer efficiency of conventional transfer schemes INEPT (18), CRIPT (19), and CRINEPT (7).

The optimal control methods for the transfer from  $I_z$  to  $2I_zS_z$  in the presence of cross-correlated relaxation immediately extend to other routinely used transfers, such as in-phase to in-phase transfer ( $I_x \rightarrow S_x$ ) (24) and single-transition to single-transition transfer (e.g.,  $2I_xS^\beta \rightarrow 2I^\beta S_x$ ) (4). Because the operators  $I_z$ ,  $S_z$ , and  $2I_zS_z$  do not decay, the optimal efficiency for the transfer  $I_x$  to  $S_x$  is achieved by first rotating  $I_x$  to  $I_z$  (which can be done rapidly with negligible loss). Then  $I_z$  is transferred optimally to  $2I_zS_z$  with efficiency  $\eta$  (Eq. 5), followed by the optimal transfer of  $2I_zS_z$  to  $S_z$ , which is finally rotated rapidly to  $S_x$ . The optimal transfer  $2I_zS_z \rightarrow S_z$  is analogous to the optimal transfer  $I_z \rightarrow 2I_zS_z$ . The efficiency  $\eta'$  for this transfer is also given by Eq. 5, where the rates  $k_a$  and  $k_c$  are replaced by the corresponding rates  $k'_a = k_{DD} + k_{CSA}^S$  and  $k'_c = k_{DD/CSA}^S$  for spin  $S$  and  $\zeta$  is replaced by the corresponding  $\zeta'$ . The maximal efficiency for the

transfer  $I_x \rightarrow S_x$  is the product of the efficiencies of the individual steps (see Table 1).

In the light of increasing use and superiority of transverse relaxation-optimized spectroscopy (TROSY) methods (4), the single-transition to single-transition transfer  $2I_xS^\beta \rightarrow 2I^\beta S_x$  is important in NMR applications to structural biology. It is of both theoretical and practical interest to establish the physical limits for this transfer. This transfer can be achieved optimally as a sequence of the following steps. First, the term  $2I_xS^\beta$  is rapidly rotated to  $2I_zS^\beta = I_z - 2I_zS_z$ . In a second step,  $-2I_zS_z$  is transferred by means of CROP to  $S_z$ , followed by the CROP transfer of  $I_z$  to  $-2I_zS_z$ . This completes the transfer from  $2I_xS^\beta$  to  $2I^\beta S_z$ , which is finally rapidly rotated to  $2I^\beta S_x$ . The maximal overall transfer efficiency is given by  $\sqrt{\eta^2 + \eta'^2}$  (cf. Table 1).

### Experimental Results

The performance of the analytically derived CROP sequences was tested experimentally by using the coupled two-spin system of  $^{13}\text{C}$ -labeled sodium formate with a coupling of  $J = 193.6$  Hz between the  $^{13}\text{C}$  spin (denoted  $I$ ) and the  $^1\text{H}$  spin (denoted  $S$ ). Sodium formate was dissolved in a mixture of 96% ( $^2\text{H}_8$ )glycerol and 4%  $^2\text{H}_2\text{O}$ . The viscosity of this solvent can be conveniently adjusted by varying the temperature. The experiments were performed at a temperature of 256.5 K, where  $k_a/J \approx 1.1$  (Fig. 5A), and 260 K, where  $k_a/J \approx 0.6$  (Fig. 5B). At a magnetic field of 17.6 T, the experimentally determined ratio of cross- to autocorrelation rate was  $k_c/k_a \approx 0.75$ . In the preparation phase of the experiments, the thermal equilibrium  $^1\text{H}$  magnetization was dephased by applying a  $90^\circ$  proton pulse followed by a pulsed

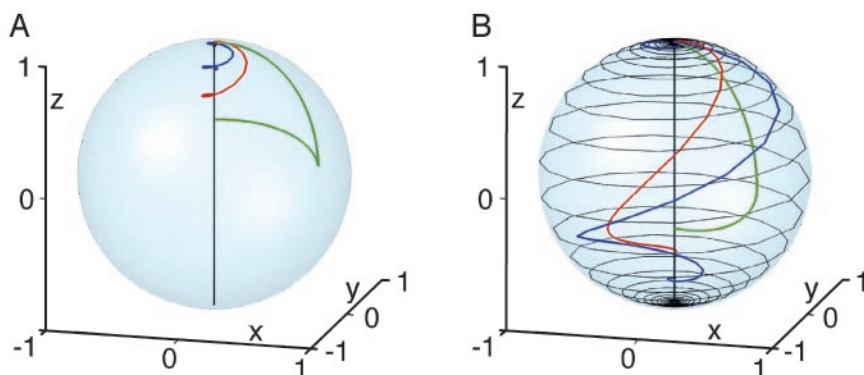


**Fig. 3.** Optimal trajectories of the expectation values of the two multiplet components  $\bar{I}S^\alpha$  (A) and  $\bar{I}S^\beta$  (B) for  $k_a = J$  and  $k_c/k_a = 0$  (green curves),  $k_c/k_a = 0.75$  (red curves),  $k_c/k_a = 0.95$  (blue curves), and  $k_c/k_a = 0.999$  (black curves).

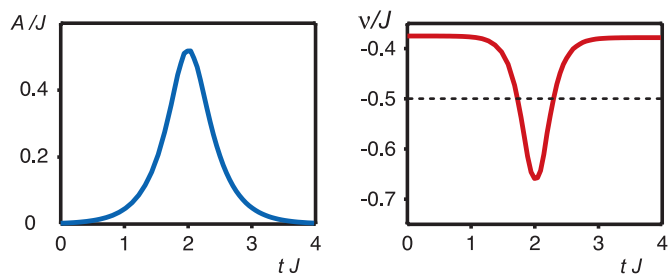


**Fig. 4.** Truncated CROP for  $k_c/k_a = 0.75$  and  $k_a = J$ . (Left) The dimensionless rf amplitude  $A/J$  with  $A = \gamma B_1/(2\pi)$  as a function of the dimensionless time  $t/J^{-1} = tJ$ . (Right) The dimensionless irradiation frequency  $\nu/J$ . The dotted line corresponds to the frequency of the narrow multiplet component that is inverted by the CROP sequence.

magnetic field gradient. The transfer efficiency of  $^{13}\text{C}$  polarization  $I_z$  to  $2I_zS_z$  was measured for the novel CROP sequence, as well as for INEPT (18), CRIPT (19), and CRINEPT (7) sequences. Finally, a hard  $90^\circ$  proton pulse was applied to transform  $2I_zS_z$  to  $2I_zS_x$ , and the amplitude of the resulting proton antiphase signal was measured. The resulting experimental transfer amplitudes are shown in Fig. 5 as a function of the transfer time. CROP sequences were truncated symmetrically to acquire transfer amplitudes also for finite mixing times. Experimentally, the optimal transfer time of the CROP sequence was found to be 7.5 ms and 15 ms, respectively. This is a compromise between losses due to the truncation of the (very long) CROP sequence and losses due to the nonzero relaxation rates of the terms  $I_zS_z$ . The experimentally determined relaxation time of these terms was about 45 ms and 80 ms, respectively. Despite these nonidealities of the model system, the CROP sequences are substantially more efficient than the conventional sequences. In Fig. 5, the experimental gains compared with CRINEPT are 34% and 22%, respectively. Although the optimal pulse sequences were designed for specific rates  $k_a$  and  $k_c$ , they were found to be robust to variations in these parameters.

## Conclusion

Here, we derived upper achievable physical limits on the efficiency of coherence and polarization transfer for two coupled spins in the presence of very general decoherence mechanisms that include cross-correlated relaxation. In this article, the focus was on the study of polarization and coherence transfer between an isolated pair of scalar coupled heteronuclear spins in the spin diffusion limit. For this example, transfer schemes were found that yield substantial gains (of up to 100%) in transfer efficiency over conventional methods. With these physical limits established, it is expected that significant improvement can be achieved over state-of-the-art experiments in protein NMR spectroscopy. Further work is necessary to incorporate practical considerations such as broadbandness and robustness with respect to variations of relaxation rates and experimental imperfections. The methods presented here can be generalized for finding relaxation-optimized pulse sequences in larger spin

**Table 1. Bounds on coherence and polarization transfer**

Transfer	Physical limits of efficiency
$I_z \rightarrow 2I_zS_z$	$\eta = \sqrt{1 + \zeta^2} - \zeta$
$2I_zS_z \rightarrow S_z$	$\eta' = \sqrt{1 + \zeta'^2} - \zeta'$
$I_z \rightarrow S_z$	$\frac{\eta\eta' + \zeta\zeta'}{\sqrt{\eta^2 + \eta'^2}}$
$I_xS^\beta \rightarrow I^\beta S_x$	$\frac{\eta\eta' + \zeta\zeta'}{\sqrt{\eta^2 + \eta'^2}}$

where  $\zeta = \sqrt{(k_a^2 - k_c^2)/(J^2 + k_c^2)}$ ,  $k_a = k_{DD} + k_{CSA}^I$ ,  $k_c = k_{DD}^I/k_{CSA}^I$ , and  $\zeta' = \sqrt{(k_a'^2 - k_c'^2)/(J^2 + k_c'^2)}$ ,  $k_a' = k_{DD} + k_{CSA}^S$ ,  $k_c' = k_{DD}^S/k_{CSA}^S$ .

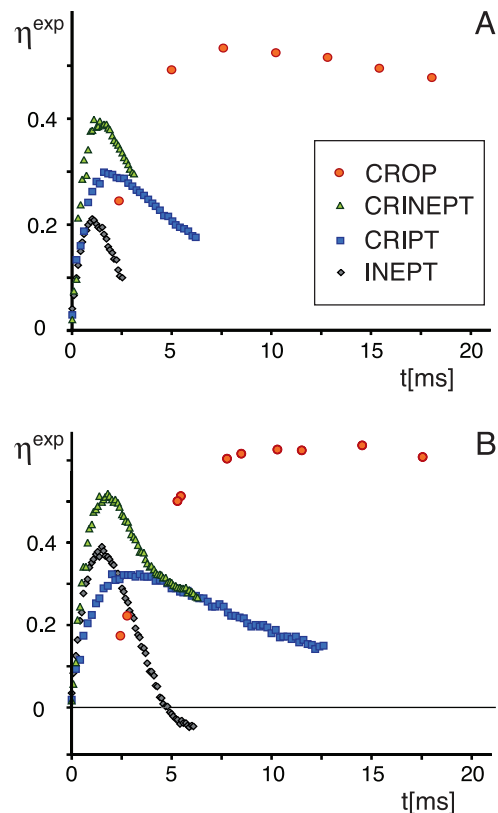


**Fig. 5.** Relative experimental transfer amplitudes of truncated CROP sequences (circles) compared with CRINEPT (triangles; ref. 7), CRIPT (squares; ref. 19), and INEPT (diamonds; ref. 18) as a function of total transfer time. The experiments were performed at a temperature of 256.5 K (A) or 260 K (B). The absolute transfer efficiencies are approximate and have been estimated on the basis of comparison with theoretical transfer curves for  $k_a/J \approx 1.1$  (A) and  $k_a/J \approx 0.6$  (B).

systems as commonly encountered, e.g., in backbone and side-chain assignments in protein NMR spectroscopy. Furthermore, these methods directly extend to other routinely used experiments such as excitation of multiple quantum coherence (2, 25, 26).

The most surprising aspect of the presented results is that despite large relaxation rates, it is possible to exploit the structure of relaxation and have decoherence-free evolution by steering the system through a decoherence-free subspace (when  $k_c = k_a$ , the operators  $I_xS^\beta$ ,  $I_yS^\beta$ , and  $I_zS^\beta$  span a decoherence-free subspace). Decoherence-free subspaces (DFS) have generated considerable interest in the area of quantum information processing recently. It has been shown that by encoding qubits within the subspaces of the Hilbert space that do not decohere, it is possible to perform error-free quantum computations (27). Interference effects among various decoherence mechanisms (13, 28) provide a way for creating DFS. It is possible that in some future implementations of quantum computing devices, by suitably engineering interference between various decoherence mechanisms, a DFS can be synthesized for error-free computation. The methods presented here can be extended to find optimal pulse sequences that in the presence of relaxation will produce a Liouville evolution that is closest to a desired unitary evolution. Such relaxation-optimized implementations of unitary propagators can then be used to minimize decoherence losses in quantum information processing.

This work was funded by Defense Advanced Research Planning Agency Grant 496020-01-1-0556, National Science Foundation Quantum and

1. Carnot, S. (1824) *Réflexions sur la Puissance Motrice du Feu* (Bachelier, Paris); trans. Fox, R. (1986) *Reflections on the Motive Power of Fire* (Barber, New York).
2. Ernst, R. R., Bodenhausen, G. & Wokaun, A. (1987) *Principles of Nuclear Magnetic Resonance in One and Two Dimensions* (Clarendon, Oxford).
3. Glaser, S. J., Schulte-Herbrüggen, T., Sieveking, M., Schedletzky, O., Nielsen, N. C., Sorensen, O. W. & Griesinger, C. (1998) *Science* **280**, 421–424.
4. Pervushin, K., Riek, R., Wider, G. & Wüthrich, K. (1997) *Proc. Natl. Acad. Sci. USA* **94**, 12366–12371.
5. Salzmänn, M., Pervushin, K., Wider, G., Senn, H. & Wüthrich, K. (1998) *Proc. Natl. Acad. Sci. USA* **95**, 13585–13590.
6. Wüthrich, K. (1998) *Nat. Struct. Biol.* **5**, 492–495.
7. Riek, R., Wider, G., Pervushin, K. & Wüthrich, K. (1999) *Proc. Natl. Acad. Sci. USA* **96**, 4918–4923.
8. McConnell, H. M. (1956) *J. Chem. Phys.* **25**, 709–711.
9. Shimizu, H. (1964) *J. Chem. Phys.* **40**, 3357–3364.
10. Ayscough, P. B. (1967) *Electron Spin Resonance in Chemistry* (Methuen, London).
11. Vold, R. R. & Vold, R. L. (1978) *Prog. NMR Spectrosc.* **12**, 79–133.
12. Goldman, M. (1984) *J. Magn. Reson.* **60**, 437–452.
13. Kumar, A., Grace, R. C. R. & Madhu, P. K. (2000) *Prog. NMR Spectrosc.* **37**, 191–319.
14. Alicki, R. & Lendi, K. (1987) *Quantum Dynamical Semigroups and Applications*, Lecture Notes in Physics (Springer, Berlin), Vol. 286.
15. Khaneja, N., Reiss, T., Luy, B. & Glaser, S. J. (2003) *J. Magn. Reson.* **162**, 311–319.
16. Pontryagin, L. S., Boltyanskii, V. G., Gamkrelidze, R. V. & Mishchenko, E. F. (1962) *The Mathematical Theory of Optimal Processes* (Interscience, New York).
17. Bryson, A. E., Jr., & Ho, Y. C. (1975) *Applied Optimal Control* (Taylor & Francis, Philadelphia).
18. Morris, G. A. & Freeman, R. (1979) *J. Am. Chem. Soc.* **101**, 760–762.
19. Brüschweiler, R. & Ernst, R. R. (1992) *Chem. Phys.* **96**, 1758–1766.
20. Hoffman, R. A. & Forsén, S. (1966) *Prog. NMR Spectrosc.* **1**, 15–204.
21. Pachler, K. G. R. & Wessels, P. L. (1973) *J. Magn. Reson.* **12**, 337–339.
22. Freeman, R. & Wittekoek, S. (1969) *J. Magn. Reson.* **1**, 238–276.
23. Freeman, R., Wittekoek, S. & Ernst, R. R. (1970) *J. Chem. Phys.* **52**, 238–276.
24. Burum, D. P. & Ernst, R. R. (1980) *J. Magn. Reson.* **39**, 163–168.
25. Aue, W. P., Bartholdi, E. & Ernst, R. R. (1976) *J. Chem. Phys.* **64**, 2229–2246.
26. Bodenhausen, G. (1981) *Prog. NMR Spectrosc.* **14**, 137–173.
27. Barenco, A., Berthiaume, A., Deutsch, D., Ekert, A., Jozsa, R. & Macchiavello, C. (1997) *SIAM J. Comp.* **26**, 1541–1557.
28. Werbelow, L. G. & Thevand, A. (1993) *J. Magn. Reson. A* **105**, 88–89.